Journal of Sol-Gel Science and Technology (2024) 109:215–225
https://doi.org/10.1007/s10971-023-06260-1

ORIGINAL PAPER

Sol-gel synthesis, characterization, and electrochemical evaluation of magnesium aluminate spinel nanoparticles for high-capacity hydrogen storage

Abbas Eslami[1] · Salahaddin Abdollah Lachini[1] · Maryam Shaterian[2] · Maryam Karami[2] · Morteza Enhessari[3]

Received: 17 August 2023 / Accepted: 31 October 2023 / Published online: 17 November 2023

Abstract

In this research, we successfully synthesized magnesium aluminate ($MgAl_2O_4$) spinel nanoparticles using a sol-gel process, with stearic acid serving as a capping agent. The synthesis process involved calcination at 900 °C for 4 h, resulting in the formation of nanoparticles with an average crystallite size of approximately 12 nm, as determined through Debye–Scherrer analysis and X-ray diffraction (XRD) data. The optical band gap was measured as 2.84 eV using Diffuse Reflectance Spectroscopy (DRS) analysis. Additionally, we found the mean pore size of the nanoparticles to be 20.2 nm through Brunauer–Emmett–Teller (BET) analysis. We characterized the resulting powders using various techniques, including Fourier Transform Infrared (FTIR) spectroscopy, Field Emission Scanning Electron Microscopy (FESEM), Energy-Dispersive X-ray Spectroscopy (EDS), and Vibrating Sample Magnetometry (VSM). We conducted electrochemical investigations utilizing the Chronopotentiometry (CP) technique. The electrochemical analysis demonstrated that $MgAl_2O_4$ spinel nanoparticles exhibit a noteworthy hydrogen storage capacity of 4000 mAh/g, highlighting their potential as promising candidates for hydrogen storage applications. This comprehensive study underscores the successful synthesis, thorough characterization, and exceptional electrochemical performance of $MgAl_2O_4$ spinel nanoparticles, firmly positioning them as valuable materials for advancing hydrogen storage technologies.

Graphical Abstract

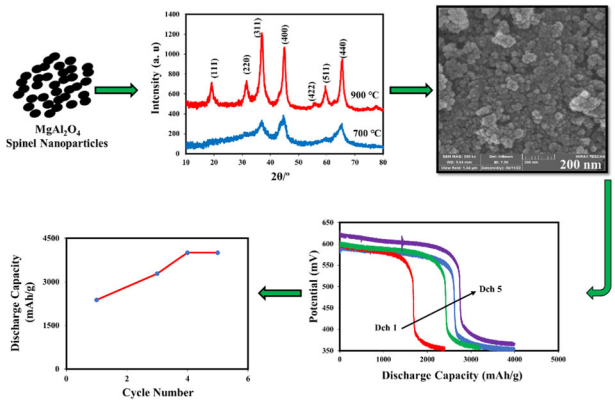

✉ Morteza Enhessari
enhessari@zedat.fu-berlin.de

[1] Department of Inorganic Chemistry, Faculty of Chemistry, University of Mazandaran, P.O. Box 47416-95447, Babolsar, Iran

[2] Department of Chemistry, Faculty of Science, University of Zanjan, Zanjan, Iran

[3] Fachbereich Biologie, Chemie, Pharmazie, Institut für Chemie und Biochemie—Anorganische Chemie, Freie Universität Berlin, Fabeckstr. 34/36, 14195 Berlin, Germany

Keywords $MgAl_2O_4$ · Nanoparticles · Sol-gel · Stearic acid · Hydrogen storage

Highlight

- $MgAl_2O_4$ spinel nanoparticles were synthesized using the gel stearic acid method.
- The structural properties were studied by various microscopic and electrochemical methods.
- $MgAl_2O_4$ spinel nanoparticles showed an excellent hydrogen storage capacity of 4000 mAh/g.

1 Introduction

The rapid growth of fossil fuel consumption and the increase in human society have led to a rise in environmental pollution and heightened concerns about the future of the planet [1]. Furthermore, the amount and type of energy used plays a significant role in daily human activities and the future. Therefore, one safe and effective way to reduce environmental pollution is to utilize green energies, renewable sources, and clean fuels like hydrogen [2]. To achieve this goal, research is currently being conducted on the production of hydrogen from renewable energy sources [3]. Hydrogen can serve as an energy carrier due to its characteristics, such as renewability, high energy content, and efficient energy conversion [4]. Hydrogen has the potential for use in various industries, including steel production, hybrid cars, engine fuel, and fuel cells [5, 6]. Notably, hydrogen is the lightest and most abundant element in the universe. When compared to other fossil fuels, such as gasoline, hydrogen boasts a higher energy density by volume and is typically stored in large tanks [7]. Hydrogen must be stored efficiently, safely, and cost-effectively. Hydrogen can be stored both chemically and physically. Storing hydrogen in nanomaterials is often based on physical absorption [8]. Several types of materials have been used to store hydrogen, such as transition mixed metal oxides [9], polymers [10], metal-organic frameworks (MOFs) [11], and graphene nanocomposites [12]. Nanoparticles are superior to other materials for hydrogen storage due to their high surface-to-volume ratio, structural stability during physicochemical reactions, small size for absorbing and releasing hydrogen molecules, and reversible storage potential [13]. Hydrogen storage in solid-state materials is one of the safest and most effective methods for storage [14].

So far, many spinel oxides have been synthesized by different methods like, $NiCr_2O_4$ [15], $NiAl_2O_4$ [16], and $MgCr_2O_4$ [17]. Previous reports have proven that spinels, such as $BaAl_2O_4$ and $CoAl_2O_4$ have been used in hydrogen storage [18, 19]. Among the spinels, magnesium aluminate spinel ($MgAl_2O_4$) has been the focus of researchers due to its excellent physicochemical properties, such as electrochemical, dielectric, thermal, mechanical, and optical properties. $MgAl_2O_4$ has been extensively studied in various forms, like nanocomposites and nanoparticles, for applications in energy storage [20–22]. Furthermore, when $MgAl_2O_4$ is combined with other materials, like metal oxides, it leads to the formation of new nanostructures that have the potential to be applied in hydrogen storage [23]. One of the best advantages of magnesium aluminate oxide compared to other materials for hydrogen storage is its high specific surface area and porous structure, which results in the formation of numerous active sites for hydrogen absorption [24]. Magnesium aluminate has a broad range of applications such as hydrogen production [25], humidity sensors [26], catalysts [27], and supercapacitors [21]. $MgAl_2O_4$ has been synthesized using various methods, including sol-gel [28], Co-precipitation [29], hydrothermal [27], solution combustion [30], and solid-state [31].

The sol-gel method for preparing magnesium aluminate spinel ($MgAl_2O_4$) offers distinct advantages over alternative methods. This method ensures high purity, employing pure metallic precursors and minimizing impurities in the final material. Additionally, sol-gel-derived $MgAl_2O_4$ typically requires lower sintering temperatures, which enhances energy efficiency and preserves material properties. The technique also allows for precise dopant control, enabling uniform incorporation of ions to tailor material properties for specific applications [15, 32, 33].

In this work, $MgAl_2O_4$ spinel nanoparticles were synthesized via a sol-gel process, using stearic acid as a capping agent for the first time. Stearic Acid, with its long carbon chain, effectively prevents nanoparticle agglomeration. Magnesium aluminate was investigated by different techniques such as XRD, FTIR, FESEM, EDS, DRS, VSM, and BET. Hydrogen storage capacity and various parameters like copper sheet surface, cycle number, and current intensity were studied. The results revealed that $MgAl_2O_4$ nanoparticles could be a promising material for hydrogen storage.

2 Experimental

2.1 Materials and methods

Aluminum nitrate ($Al(NO_3)_3{\cdot}9H_2O$), magnesium acetate (with better solubility and more stability) ($Mg(OAc)_2{\cdot}4H_2O$), and stearic acid ($C_{18}H_{36}O_2$) with 99.9% purity were purchased from Merck. The XRD patterns of

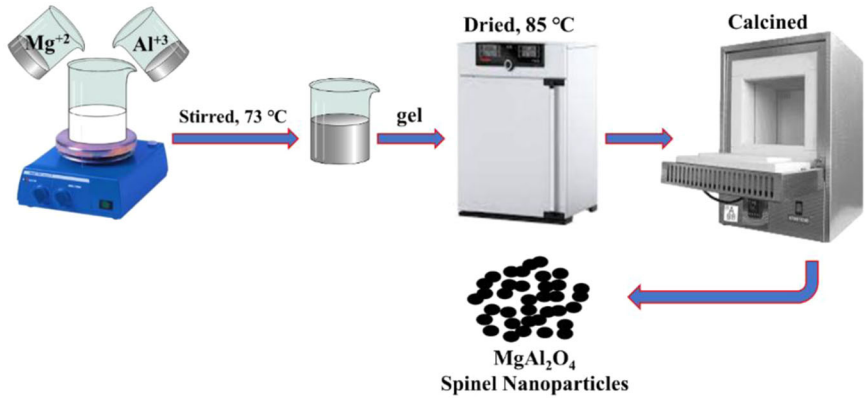

Scheme. 1 Schematic diagram of synthesized $MgAl_2O_4$ spinel NPs

Table. 1 The elementary components of $MgAl_2O_4$ spinel NPs at 900 °C

Element	Mg	Al	O	Total
W (%)	19.83	48.31	31.86	100
Mole fraction	0.15	0.3	0.55	1

$MgAl_2O_4$ nanoparticles were analyzed by a Model PTS 3003 SEIFERT diffractometer using Cu Kα radiation (λ = 1.54 Å) and in the 2θ range from 10° to 80° to study the structural development and crystallization of the sample. The FTIR spectrum of the $MgAl_2O_4$ nanoparticles was recorded with an MB100 (BOMEM) spectrophotometer using a KBr pellet. FESEM was used to investigate the size distribution and surface morphology of the samples (JEOL-64000, Japan). The energy dispersive spectrometry (EDS) evaluation was performed by Philips EM208. To study the magnetic properties of the sample, a Vibrating Sample Magnetometer was used (Meghnatis Daghigh Kavir Co., Kashan, Iran). The band gap of the sample was determined through UV absorption spectra (Shimadzu UV/3101 PC) within a wavelength range of 300 to 500 nm. Brunauer–Emmett–Teller (BET) specific surface areas of the catalysts were determined through N2 adsorption/desorption tests performed on an ASAP-2010 analyzer (Micromeritics, USA). The chronopotentiometry method was applied to estimate the discharge capacity (hydrogen storage capacity) of a sample using the SAMA 500 electro-analyzer system in Iran (potentiostat/galvanostat).

2.2 Preparation of $MgAl_2O_4$ spinel Nanoparticles

$MgAl_2O_4$ spinel nanoparticles (NPs) were prepared via the sol-gel process, using Magnesium acetate, Aluminum nitrate as the cation source, and stearic acid as a capping agent. First, 10 mmol stearic acid was melted in a beaker at 73 °C. Then, 1 mmol magnesium acetate and 2 mmol aluminum nitrate were dissolved in distilled water (pH = 4). The solutions containing metallic ions were added to stearic acid and stirred at a temperature of 65–85 °C to form a viscous gel. After cooling the gel at room temperature, it was heated in an electric oven at 85 °C for 24 h to dry. During this time, metal cations diffusion from the aqueous phase to the organic phase, resulting in a homogeneous sol. Finally, the dried gel was calcined at temperatures of 700 and 900 °C for 4 h to obtain $MgAl_2O_4$ spinel nanoparticles. Scheme 1. displays a schematic diagram of synthesized $MgAl_2O_4$ spinel NPs at temperatures of 700 and 900 °C for 4 h (Table 1).

2.3 Electrochemical hydrogen storage

The chronopotentiometry method is a significant technique for estimating the hydrogen storage capacitance. In this electrochemical cell, Ag/AgCl, Pt, and Cu-$MgAl_2O_4$ are the reference, counter (anode), and working (cathode or coated-copper plate) electrodes, respectively. The electrolyte is 6 M KOH aqueous solution. In this system, a current intensity (±1 mA) is applied between the counter (anode) and working (cathode) electrodes, and the potential differences are estimated between the working and the Ag/AgCl (reference) electrodes. To fabricate an electrode of Cu-$MgAl_2O_4$, the copper sheet used as a thin substrate for the Cu/$MgAl_2O_4$. The $MgAl_2O_4$ powder is sonicated in ethanol for 10 min. A pure copper sheet ($1 \times 1\ cm^2$) is coated by a substrate of $MgAl_2O_4$ powder at 100 °C [13].

3 Results and discussion

3.1 XRD analysis

XRD diffractograms of $MgAl_2O_4$ spinel nanoparticles calcined at temperatures of 700 and 900 °C for 4 h in the 2θ range from 10º–80º are illustrated in Fig. 1a. As can be seen in Fig. 1a, the XRD pattern of $MgAl_2O_4$ calcined at 700 °C demonstrated weak peaks with low intensity. Therefore, it can be concluded that the primary structure of these

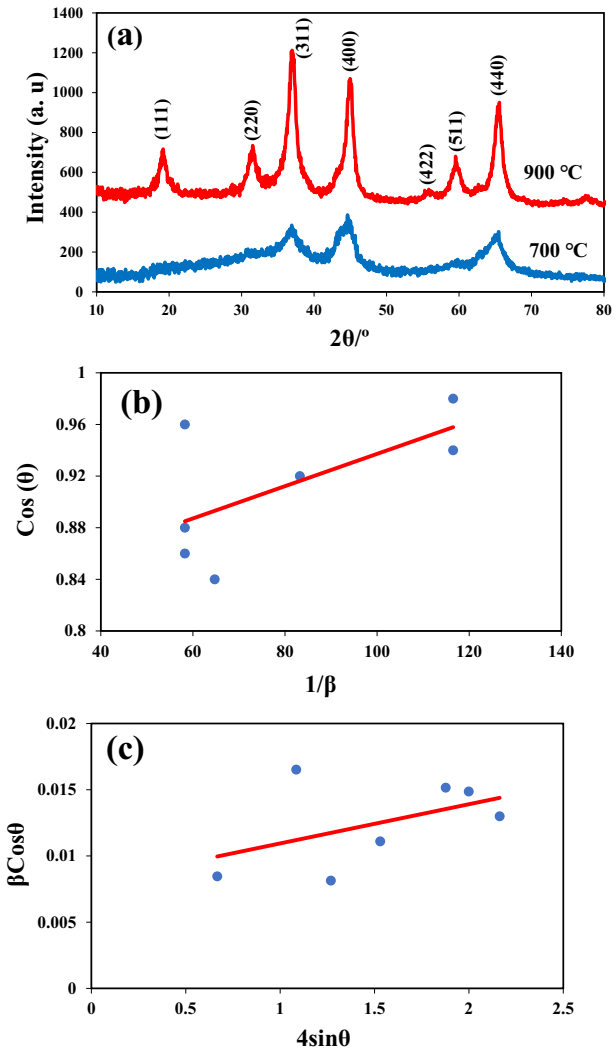

Fig. 1 **a** XRD diffractogram of synthesized $MgAl_2O_4$ (**b**) Debye–Scherrer plot, (**c**) Williamson-Hall plot

nanoparticles is being formed, and crystals have not yet grown completely at 700 °C. An increase in temperature up to 900 °C leads to an increase in the size of the crystals, resulting in broadened diffraction peaks. All diffraction peaks at 2θ values of 19°, 31°, 37°, 45°, 56°, 59.6° and 65.5° can be indexed (111), (220), (311), (400), (422), (511), and (440) crystal planes, respectively. The results exhibited that $MgAl_2O_4$ (JCPDS- 01-071-2499) has a cubic crystal structure with space group Fd-3m and lattice parameters a = b = c = 8.05Å. No detected impurities like MgO or Al_2O_3. The average crystallite size of the $MgAl_2O_4$ spinel nanoparticles calcined at 900 °C for 4 h was calculated from the XRD diffractogram utilizing the Debye–Scherrer relation (Eq. 1) [34]:

$$D = \frac{k\lambda}{\beta \operatorname{Cos}\theta} \tag{1}$$

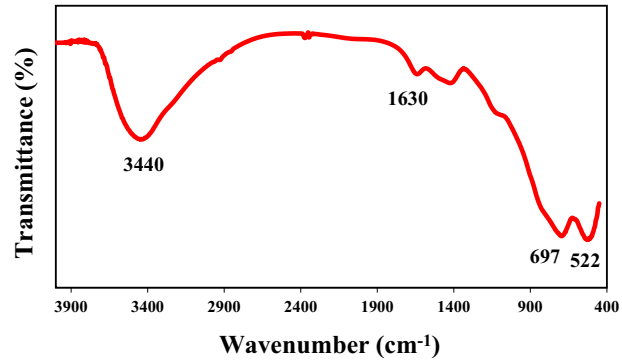

Fig. 2 FTIR spectroscopy of synthesized $MgAl_2O_4$ spinel NPs at 900 °C

Where β is the width of the XRD peak at half height, k is a shape factor of about 0.9 for spherical-shaped nanoparticles, D is the mean particle diameter, λ is the wavelength (0.15418 nm), and θ is the diffraction angle. The average crystallite size was calculated utilizing the linear fit of Eq. 1 to the plot cosθ vs 1/β depicted in Fig. 1b. The average crystal size was estimated to be 12 nm (increasing temperature = promoting crystal growth) [35]. The Debye −Scherrer equation calculates the crystallite size without considering lattice distortion and micro-strain induced in the structure. Therefore, the Williamson-Hall (W-H) relation was used to analyze the effect of lattice on strain the peak broadening [36, 37] (Eq. 2):

$$\beta \cos\theta = \frac{k\lambda}{D} + 4\varepsilon \sin\theta \tag{2}$$

Where ε is the strain induced in the lattice, and D is the average crystallite size. According to Fig. 1c, the lattice strain and crystallite size have been calculated using the Williamson-Hall plot. Figure 1c displays the fit of Eq. 2 to the β cos θ vs 4 sin θ plot. The average crystallite size and lattice strain were estimated by determining the intercept and slope of the graph, these were found to be 17.35 nm and 296×10^{-5}, respectively. The crystallite size obtained by the Williamson-Hall equation is slightly larger than that calculated by the Debay-Scherrer equation. This difference may be due to considering the strain impact as calculated by the Williamson-Hall equation [38] (Fig. 2).

3.2 FT-IR spectroscopy

The results of FT-IR spectroscopy for $MgAl_2O_4$ spinel NPs at 900 °C are shown in Fig. 2. Two absorption bonds can be seen at 522–697 cm^{-1}, which are attributed to the vibrations involving metal-oxygen bondssuch as Al-O stretching in the AlO_6 group and lattice vibration of Mg-O stretching [28, 39]. The vibration bond observed at 1630 cm^{-1} is related to bending (H-O-H), and the vibration band around 3440 cm^{-1} corresponds to the OH group [40].

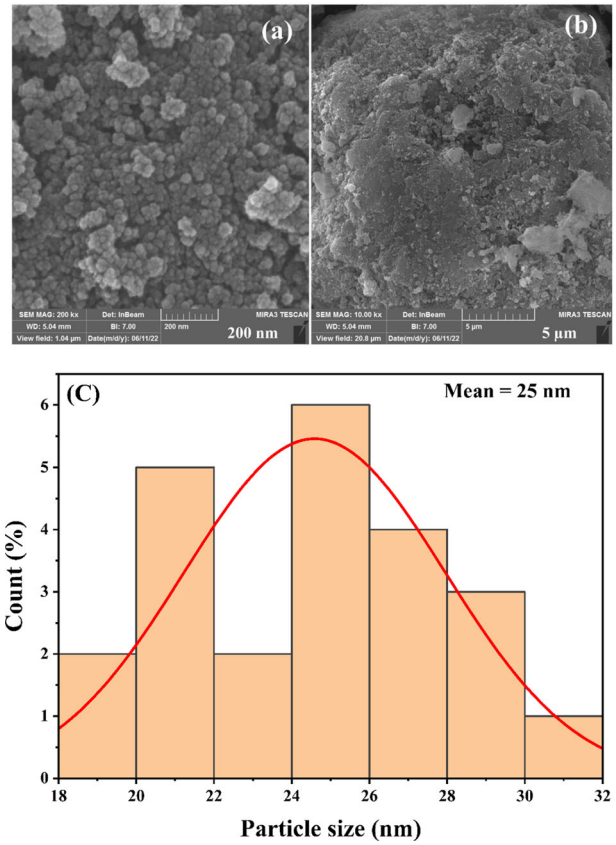

Fig. 3 FESEM images (**a**, **b**), particle size distribution (**c**) of synthesized $MgAl_2O_4$ spinel NPs at 900 °C

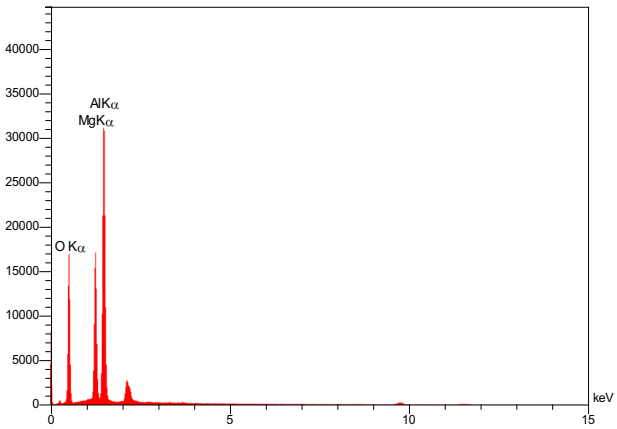

Fig. 4 EDS spectrum of $MgAl_2O_4$ NPs at 900 °C

3.3 FESEM and energy dispersive X-ray (EDS)

The surface morphology of the $MgAl_2O_4$ spinel NPs calcined at 900 °C was studied using FESEM analysis. The FESEM images of the sample are displayed in Fig. 3a, b. The powder sample showed the formation of uniform spherical shapes and homogeneity of the structure. Furthermore, the FESEM images of the $MgAl_2O_4$ spinel nanoparticles was analyzed using the ImageJ software [39]. The histogram plot of the sample is shown in Fig. 3c. The average grain size was obtained 25 nm. The EDX spectrum of the $MgAl_2O_4$ spinel nanoparticles is depicted in Fig. 4. The EDS results demonstrate the presence of oxygen, aluminum, and magnesium elements without impurity. The elementary constituents of $MgAl_2O_4$ spinel NPs are displayed in Table 1 [41, 42].

3.4 Optical properties

The energy gap (Eg) and absorption coefficient are desirable features of semiconductors that determine their applications in optoelectronics. The results of the UV–vis absorption spectrum of $MgAl_2O_4$ spinel NPs in the wavelength range of 300–500 nm are depicted in Fig. 5a, b. The absorption peak was observed at 380 nm due possibly to the $O^{2-} \rightarrow Al^{3+}$ charge transition [43]. The photon energy (E_g) has been obtained utilizing Tuac's relation (Eg) (Eq. 3).

$$(\alpha h\nu)^n = A\left(h\nu - E_g\right) \tag{3}$$

Where h is the Planck's constant ($6.62607004 \times 10^{-34}$ m^2kg/s), υ is the Frequency (Hz), α is the Absorption coefficient, A is the Energy independent constant, Eg band gap energy (eV) and n is the nature of transmission. Accordingly, the band gap energy of the nanoparticle was evaluated using a graph of $(\alpha h\nu)^2$ values against the band gap energy (hν) axis extrapolating the linear portion of the absorption edge to find the interruption by energy axis. Figure 5b shows the optical band gap of $MgAl_2O_4$ spinel nanoparticles. The value of the direct band gap for $MgAl_2O_4$ spinel nanoparticles came out to be 2.84 eV [31]. Previous reports showed that the optical reflectance of $MgAl_2O_4$ spinel nanoparticles depends on the calcination temperature [44]. As the calcination temperature is increased beyond 800 °C, the crystallite size of $MgAl_2O_4$ increases leading to a decrease in the energy of the band gap. In other words, the optical reflectance properties of $MgAl_2O_4$ spinel NPs can be attributed to its cubic crystal structure system. The reduction in bandgap energy may be due to the accumulation of defect states between the valence and conduction bands [45]. Consequently, $MgAl_2O_4$ spinel NPs can be employed as semiconductor and photocatalyst.

3.5 VSM studies

The magnetic behavior of $MgAl_2O_4$ spinel NPs has been measured (Fig. 6). The magnetic properties of the sample were observed at room temperature. Exploring the M-H curve confirms the ferromagnetic properties of $MgAl_2O_4$ spinel NPs. The ferromagnetic property of $MgAl_2O_4$ spinel NPs has already been reported [46]. The saturation

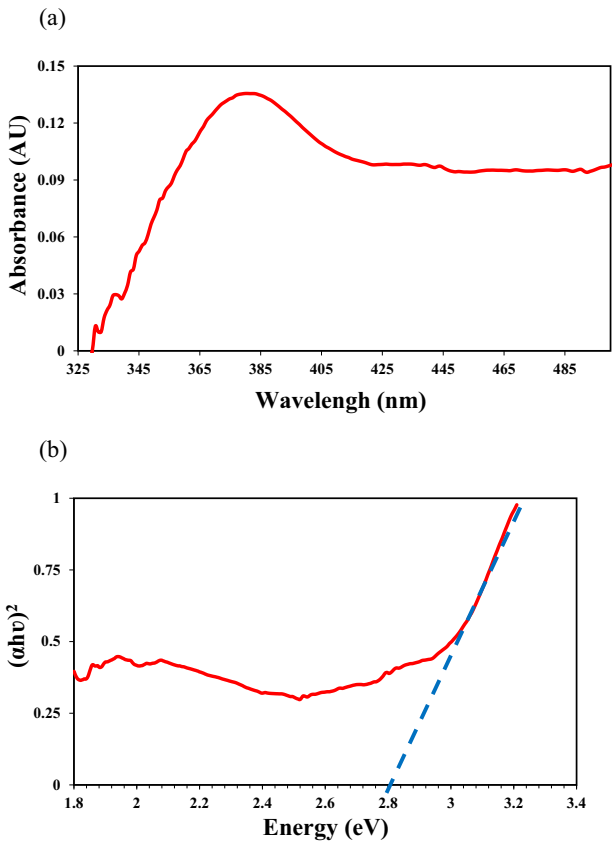

Fig. 5 **a** DRS of synthesized $MgAl_2O_4$ NPs at 900 °C. **b** The optical band gap of synthesized $MgAl_2O_4$ NPs at 900 °C

magnetization (Ms), remanence magnetization (Mr), and coercivity field (Hc) were about 0.0154 emu/g, 0.0244 emu/g, and 200 Oe, respectively. The remanence ratio (Mr/Ms) value was estimated at around 1.584. The saturation magnetization (Ms) of 0.0154 emu/g indicates their capacity for strong magnetization under an external field. This Mr value suggests notable magnetic memory after the field is removed, while the Hc of 200 Oe signifies $MgAl_2O_4$ resistance to demagnetization. The value of 1.584 highlights the (Mr/Ms) ability to maintain magnetization, showcasing the potential for applications in data storage and magnetic devices. Normal spinel, also known as cubic spinel, can exhibit ferromagnetic behavior due to the presence of magnetic ions in its crystal structure. This mineral's chemical formula is AB_2O_4, with A and B representing different metal cations. Ferromagnetism emerges from the alignment of magnetic moments of these cations within the crystal lattice. When magnetic ions occupy both the A and B sites, they interact via exchange interactions that favor parallel alignment of their magnetic moments. When a magnetic field is applied, the magnetic moments align themselves with the field, leading to saturation magnetization. Bulk normal spinel may contain magnetic domains, with

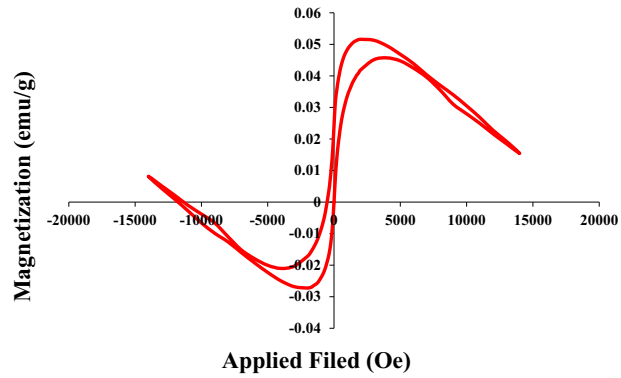

Fig. 6 M-H curve of synthesized $MgAl_2O_4$ NPs at 900 °C

groups of atomic magnetic moments aligning in the same direction. The specific combination of magnetic ions and their arrangement in the lattice, as well as temperature, determine whether ferromagnetism is observed in each normal spinel compound. Ferromagnetism in the normal spinel is a result of quantum mechanical interactions and the behavior of magnetic moments in the crystal structure.

3.6 BET technique

The specific surface region of the $MgAl_2O_4$ spinel NPs at 900 °C was estimated using a BET- BJH technique. The result is illustrated in Fig. 7a, b. The N_2 adsorption/desorption and the categorization of IUPAC demonstrate a characterization of Class IV in the adsorption isotherms with hysteresis loops [35]. The $MgAl_2O_4$ spinel NPs (which have a mesoporous structure) exhibit hysteresis of H3-type. The specific surface area of 108.1 m^2/g indicates a substantial surface area available for interactions with hydrogen molecules, suggesting a high adsorption capacity. The pore volume of 0.5459 cm^3/g is noteworthy, as it implies that the material can hold a significant amount of hydrogen gas, making it suitable for various practical applications, including hydrogen fuel cells and transportation. Furthermore, the mean pore size of 20.2 nm provides insights into the material's pore structure, which is vital for hydrogen mobility and accessibility. The diversity in pore sizes within the nanoparticles allows for accommodating different masses of hydrogen, facilitating their diffusion into and out of the material. Overall, the BET results emphasize the material's potential for gas adsorption and storage with a particular focus on hydrogen, thanks to the significant specific surface area, pore volume, and mean pore size. On the other hand, the FESEM results provide visual confirmation of the nanoparticles' size, shape, and uniformity, which can be important for applications that rely on a consistent and well-defined nanoparticle structure.

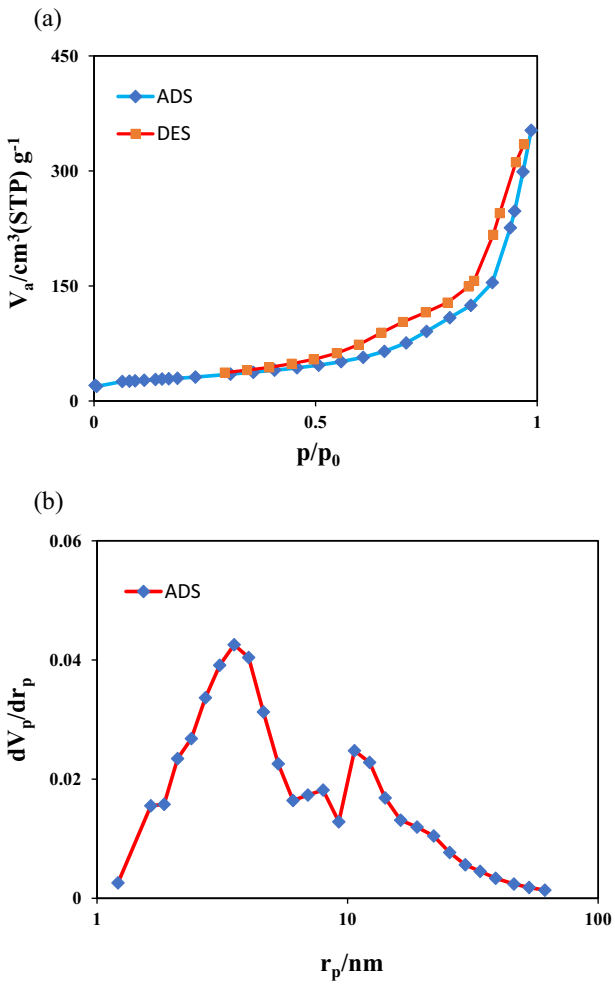

Fig. 7 **a** N_2 adsorption-desorption isotherms and (**b**) pore size distributions of the prepared sample at 900 °C

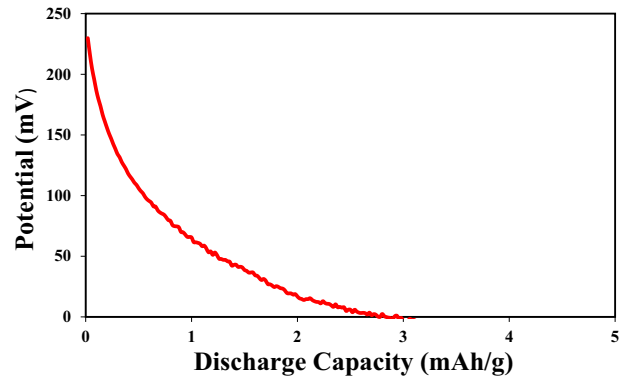

Fig. 8 The discharge capacity of copper foam without attendance $MgAl_2O_4$

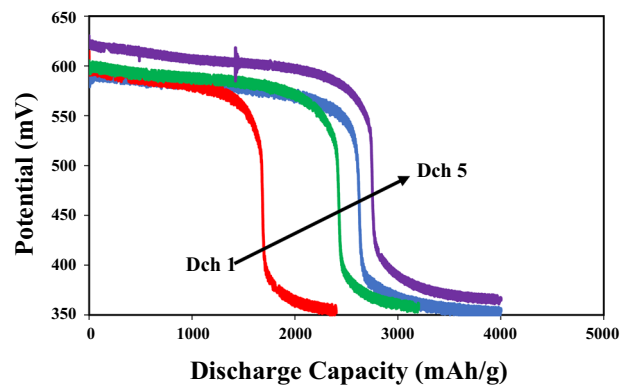

Fig. 9 The discharge properties of the Cu- $MgAl_2O_4$ electrode over the 5 cycles under a current constant 1 mA

3.7 Hydrogen storage capacity

According to Fig. 8, the discharge capacity of copper foam without $MgAl_2O_4$ attendance is almost equal to 3 mAh/g. Figure 9 illustrates the discharge properties of the Cu-$MgAl_2O_4$ electrode after 5 cycles under a constant current of 1 mA. Additionally, this diagram indicates that placing the Cu-$MgAl_2O_4$ electrode in an alkaline medium can affect its capacity. Electrochemical hydrogen absorption mechanisms occur during three reactions: Volmer, Tafel, and Heyrovsky [47]. The electrolyte solution was prepared using a 6 M KOH combination dissolved in deionized water (Proton source). As a result of the decomposition of water, H atoms are formed (Eq. 4). During the charging process (Volmer reaction), the electrolyte is separated around the working electrode, and hydrogen is adsorbed on the $MgAl_2O_4$ nanoparticles surface (Eq. 5).

$$H_2O + e^- \rightleftarrows H + OH^- \tag{4}$$

$$MgAl_2O_4 + H_2O + e^- \rightleftarrows (MgAl_2O_4 - H_{ads}) + OH^- \tag{5}$$

According to the Volmer, the reaction reduction of H_2O to hydroxyl ions and the adsorption of hydrogen atoms onto the working electrode surface; result in the formation of subsurface hydrogen (H_{ss}).

$$MgAl_2O_4 - H_{ads} \rightleftarrows MgAl_2O_4 - H_{ss} \tag{6}$$

Then, subsurface hydrogen atoms (H_{ss}) diffuse as bulk-absorbed hydrogen (H_{abs}).

$$MgAl_2O_4 - H_{ss} \rightleftarrows MgAl_2O_4 - H_{abs} \tag{7}$$

The increase of surface accumulated hydrogen causes the migration of adsorbed H (H_{ads}) into the $MgAl_2O_4$ network. During the discharge process, which occurs in the opposite direction to the charging process, the absorbed hydrogen atoms are desorbed from the surface of the working electrode and turned back into water, releasing an electron. The adsorption of hydrogen atoms on the surface of the Cu-$MgAl_2O_4$ (cathode) is a type of physical adsorption [48]. The discharge capacity enhanced from 2380 mAh/g in the first cycle to 4000 mAh/g after 5 cycles. The increase in discharge capacity can likely be explained by the formation of more active sites for hydrogen desorption/absorption on

the surface of the working electrode, the pore distribution, and the surface-to-volume ratio of $MgAl_2O_4$ spinel nanoparticles. [49]. Based on the physical adsorption equations for electrochemical hydrogen storage, such as the sidewise Tafel reaction (Eqs. 9, 10) and the Heyrovsky process (Eq. 11), if the hydrogen absorption energy is less than the released energy, gaseous hydrogen (H_2) is formed.

$$MgAl_2O_4 - H_{ads} + MgAl_2O_4 - H_{ads} \rightleftarrows 2\,MgAl_2O_4 + H_2(g) \tag{8}$$

$$H + H \rightleftarrows H_2 \tag{9}$$

$$MgAl_2O_4 - H_{ads} + H_2O + e^- \rightleftarrows MgAl_2O_4 + H2(g) + OH^- \tag{10}$$

Figure 10 shows the cycling performance of the $MgAl_2O_4$ nanoparticles at a constant current of 1 mA. The amount of stored hydrogen in the working electrode can be measured by the discharge capacity. The storage capacity (SC) can be estimated from the charge/discharge curves of the electrodes according to Eq. 11 [50].

$$\text{Storage Capacity (SC)} = [\text{Time(h)} \times \text{Current(mA)}]/\text{Active Mass}\,(g) \tag{11}$$

The $MgAl_2O_4$ spinel nanoparticles are suitable due to their fewer cycle number, low cost, and desirable electrochemical discharge capacity. Table 2 displays a comparison between $MgAl_2O_4$ spinel nanoparticles and the previously reported nanomaterials.

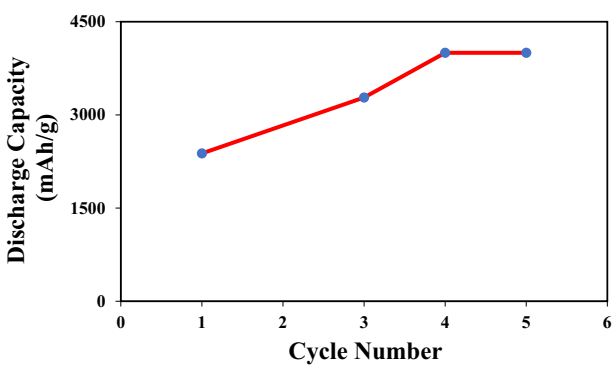

Fig. 10 Cycling effect of Cu-$MgAl_2O_4$ electrodes on the amount of storage capacity at 1 mA

4 Conclusion

In summary, $MgAl_2O_4$ spinel nanoparticles (NPs) were successfully synthesized through the sol-gel process at a temperature of 900 °C, utilizing stearic acid as a capping agent. The obtained results revealed an average crystallite size of approximately 12 nm and a specific surface area of 108.1 $m^2.g^{-1}$, both of which were associated with a mesoporous structure. The EDS and FESEM analyses confirmed the purity of the acquired $MgAl_2O_4$ spinel NPs, exhibiting a lack of impurities and showcasing a consistently small, uniform, and spherical morphology.

Furthermore, the optical band gap, calculated as 2.84 eV using Diffuse Reflectance Spectroscopy (DRS), falls within the range indicative of efficient photo-catalytic behavior. The Vibrating Sample Magnetometer (VSM) analysis indicated ferromagnetic behaviors within the nanoparticles.

Owing to their distinctive structure and properties, $MgAl_2O_4$ spinel nanoparticles hold promise for application in hydrogen energy storage. Notably, the nanoparticles demonstrated a noteworthy maximum discharge capacity of 4000 mAh/g, solidifying their potential as a suitable candidate for hydrogen storage applications.

Acknowledgements The authors of this article would like to express their gratitude and appreciation for the financial support provided by the Mazandaran University Research Council and Freie Universitat Berlin.

Author contributions In accordance with the guidelines set by the "Journal of Sol-Gel Science and Technology" we hereby provide a detailed account of the contributions made by each author to the research presented in the manuscript titled "Sol-Gel Synthesis, Characterization, and Electrochemical Evaluation of Magnesium Aluminate Spinel Nanoparticles for High-Capacity Hydrogen Storage." ME: conceptualization, methodology, supervision conceived the research idea and formulated the objectives of the study. Designed the experimental methodology for the sol-gel synthesis of magnesium aluminate spinel nanoparticles. Provided oversight and guidance throughout the research project. SAL: synthesis and characterization conducted the experimental synthesis of magnesium aluminate spinel nanoparticles using the sol-gel method. Carried out detailed characterization of the synthesized nanoparticles using techniques such as X-ray diffraction (XRD) and scanning electron microscopy (SEM).

Table 2 Comparison of the hydrogen discharge capacity of different nanomaterials

Sample	Number of Cycle	Discharge Capacity ($mAhg^{-1}$)	Ref.
$MgMn_2O_4$	5	2000	[9]
$Ca_2Mn_3O_8/CaMn_3O_6$	95	105	[51]
Fe_3O_4/G	5	900	[52]
$MgAl_2O_4$	5	4000	Current work

Analyzed the characterization data and contributed to the interpretation of the results. MS: electrochemical evaluation designed and executed the electrochemical evaluation experiments to assess the hydrogen storage capacity of the synthesized nanoparticles. Conducted cyclic voltammetry and chronoamperometry experiments and collected relevant electrochemical data. Contributed to the discussion and analysis of the electrochemical results in the context of hydrogen storage applications. MK: data analysis and interpretation compiled and organized the experimental data obtained from the synthesis, characterization, and electrochemical evaluation. Conducted statistical analysis of the data and interpreted the trends observed. Collaborated with other authors to correlate the results with the theoretical framework and the broader context of hydrogen storage materials. AE: manuscript preparation and writing drafted the initial version of the manuscript, incorporating the contributions from all authors. Ensured the manuscript adheres to the journal's formatting and citation guidelines. Integrated feedback from co-authors and revised the manuscript for clarity, coherence, and scientific accuracy. All authors have read and approved the final version of the manuscript submitted to the "Journal of Sol-Gel Science and Technology." We affirm that the work presented represents a collaborative effort where each author's expertise contributed significantly to different aspects of the research process.

FundingInformation Open Access funding enabled and organized by Projekt DEAL.

Compliance with ethical standards

Conflict of interest The authors declare no competing interests.

Publisher's note Springer Nature remains neutral with regard to jurisdictional claims in published maps and institutional affiliations.

References

1. Bilen K, Ozyurt O, Bakırcı K, Karslı S, Erdogan S, Yılmaz M, Comaklı O (2008) Energy production, consumption, and environmental pollution for sustainable development: a case study in Turkey. Renew Sustain Energy Rev 12:1529–1561. https://doi.org/10.1016/j.rser.2007.03.003
2. Sharma S, Agarwal S, Jain A (2021) Significance of hydrogen as economic and environmentally friendly fuel. Energies 14:7389. https://doi.org/10.3390/en14217389
3. Qureshi F, Yusuf M, Kamyab H, Zaidi S, Junaid Khalil M, Arham Khan M, Azad Alam M, Masood F, Bazli L, Chelliapan S, Abdullah B (2022) Current trends in hydrogen production, storage and applications in India: a review. Sustain Energy Technol Assessments 53:102677. https://doi.org/10.1016/j.seta.2022.102677
4. Orhan MF, Babu BS (2015) Investigation of an integrated hydrogen production system based on nuclear and renewable energy sources: Comparative evaluation of hydrogen production options with a regenerative fuel cell system. Energy 88:801–820. https://doi.org/10.1016/j.energy.2015.06.009
5. Liu W, Zuo H, Wang J, Xue Q, Ren B, Yang F (2021) The production and application of hydrogen in steel industry. Int J Hydrogen Energy 46:10548–10569. https://doi.org/10.1016/j.ijhydene.2020.12.123
6. Bartolucci L, Cennamo E, Cordiner S, Mulone V, Pasqualini F, Boot MA (2023) Digital twin of a hydrogen fuel cell hybrid electric vehicle: effect of the control strategy on energy efficiency. Int J Hydrogen Energy 48:20971–20985. https://doi.org/10.1016/j.ijhydene.2022.11.283
7. Tashie-Lewis BC, Nnabuife SG (2021) Hydrogen production, distribution, storage and power conversion in a hydrogen economy—a technology review. Chem Eng J Adv 8:100172. https://doi.org/10.1016/j.ceja.2021.100172
8. Chen, Y. P., Bashir, S., & Liu, J. L. (2017). Nanostructured materials for next-generation energy storage and conversion. Springer Berlin, Heidelberg, pp117–142. https://doi.org/10.1007/978-3-662-53514-1
9. Eslami A, Lachini SA, Shaterian M, Karami M, Enhessari M (2023) Synthesis, characterization, and hydrogen storage capacity of $MgMn_2O_4$ spinel nanostructures. Inorg Chem Commun 110875. https://doi.org/10.1016/j.inoche.2023.110875
10. Mahato N, Jang H, Dhyani A, Cho S (2020) Recent progress in conducting polymers for hydrogen storage and fuel cell applications. Polymers (Basel) 12:2480. https://doi.org/10.3390/polym12112480
11. Cao Y, Dhahad HA, Zare SG, Farouk N, Anqi AE, Issakhov A, Raise A (2021) Potential application of metal-organic frameworks (MOFs) for hydrogen storage: Simulation by artificial intelligent techniques. Int J Hydrogen Energy 46:36336–36347. https://doi.org/10.1016/j.ijhydene.2021.08.167
12. Deniz CU, Mert H, Baykasoglu C (2021) Li-doped fullerene pillared graphene nanocomposites for enhancing hydrogen storage: a computational study. Comput Mater Sci 186:110023. https://doi.org/10.1016/j.commatsci.2020.110023
13. Gholami T, Salavati-Niasari M, Varshoy S (2017) Electrochemical hydrogen storage capacity and optical properties of $NiAl_2O_4$/NiO nanocomposite synthesized by green method. Int J Hydrogen Energy 42:5235–5245. https://doi.org/10.1016/j.ijhydene.2016.10.132
14. Boateng E, Chen A (2020) Recent advances in nanomaterial-based solid-state hydrogen storage. Mater Today Adv 6:100022. https://doi.org/10.1016/j.mtadv.2019.100022
15. Javed M, Khan AA, Kazmi J, Mohamed MA, Khan MN, Hussain M, Bilkees R (2021) Dielectric relaxation and small polaron hopping transport in sol-gel-derived $NiCr_2O_4$ spinel chromite. Mater Res Bull 138:111242. https://doi.org/10.1016/j.materresbull.2021.111242
16. Iqbal Y, Shah WH, Khan B, Javed M, Ullah H, Khan N, Khan AR, Asghar G, Safeen A (2023) Small polaron hopping transport mechanism, dielectric relaxation and electrical conduction in $NiAl_2O_4$ electro-ceramic spinel oxide. Phys Scr 98:065951. https://doi.org/10.1088/1402-4896/acd5ba
17. Javed M, Khan AA, Ahmed MS, Khisro SN, Kazmi J, Bilkees R, Khan MN, Mohamed MA (2020) Temperature dependent impedance spectroscopy and electrical transport mechanism in sol-gel derived $MgCr_2O_4$ spinel oxide. Phys B Condens Matter 599:412377. https://doi.org/10.1016/j.physb.2020.412377
18. Gholami T, Salavati-Niasari M, Varshoy S (2016) Investigation of the electrochemical hydrogen storage and photocatalytic

properties of $CoAl_2O_4$ pigment: Green synthesis and characterization. Int J Hydrogen Energy 41:9418–9426. https://doi.org/10.1016/j.ijhydene.2016.03.144
19. Salehabadi A, Salavati-Niasari M, Sarrami F, Karton A (2017) Sol-Gel auto-combustion synthesis and physicochemical properties of $BaAl_2O_4$ nanoparticles; electrochemical hydrogen storage performance and density functional theory. Renew Energy 114:1419–1426. https://doi.org/10.1016/j.renene.2017.07.119
20. Ganesh I (2013) A review on magnesium aluminate ($MgAl_2O_4$) spinel: synthesis, processing and applications. Int Mater Rev 58:63–112. https://doi.org/10.1179/1743280412Y.0000000001
21. Alam MW, Kumar VGD, Ravikumar CR, Prashantha SC, Murthy HCA, Kumar MRA (2022) Chromium (III) doped polycrystalline $MgAl_2O_4$ nanoparticles for photocatalytic and supercapacitor applications. J Phys Chem Solids 161:110491. https://doi.org/10.1016/j.jpcs.2021.110491
22. Ullah F, Qureshi MT, Sultana K, Saleem M, Al Elaimi M, Abdel Hameed R, ul Haq S, Ismail HS, Anwar MS (2021) Structural and dielectric studies of $MgAl_2O_4$–TiO_2 composites for energy storage applications. Ceram Int 47:30665–30670. https://doi.org/10.1016/j.ceramint.2021.07.244
23. Zeng D-W, Peng S, Chen C, Zeng J-M, Zhang S, Zhang H-Y, Xiao R (2016) Nanostructured Fe_2O_3/$MgAl_2O_4$ material prepared by colloidal crystal templated sol–gel method for chemical looping with hydrogen storage. Int J Hydrogen Energy 41:22711–22721. https://doi.org/10.1016/j.ijhydene.2016.09.180
24. Wang F, Luo M, Liu Q, Shao C, Yang Z, Liu X, Guo J (2023) Preparation of Pt/$MgAl_2O_4$ decalin dehydrogenation catalyst for chemical hydrogen storage application. Catal Lett 1–15. https://doi.org/10.1007/s10562-023-04283-5
25. Gómez-Solís C, Peralta-Arriaga SL, Torres-Martínez LM, Juárez-Ramírez I, Díaz-Torres LA (2017) Photocatalytic activity of MAl_2O_4 (M = Mg, Sr and Ba) for hydrogen production. Fuel 188:197–204. https://doi.org/10.1016/j.fuel.2016.10.038
26. Das S, Rahman ML, Mondal PP, Mahapatra PL, Saha D (2021) Screen-printed $MgAl_2O_4$ semi-thick film based highly sensitive and stable capacitive humidity sensor. Ceram Int 47:33515–33524. https://doi.org/10.1016/j.ceramint.2021.08.260
27. Zhang X (2009) Hydrothermal synthesis and catalytic performance of high-surface-area mesoporous nanocrystallite $MgAl_2O_4$ as catalyst support. Mater Chem Phys 116:415–420. https://doi.org/10.1016/j.matchemphys.2009.04.012
28. Milani SS, Kakroudi MG, Vafa NP, Rahro S, Behboudi F (2021) Synthesis and characterization of $MgAl_2O_4$ spinel precursor sol prepared by inorganic salts. Ceram Int 47:4813–4819. https://doi.org/10.1016/j.ceramint.2020.10.051
29. Nam S, Lee M, Kim B-N, Lee Y, Kang S (2017) Morphology controlled Co-precipitation method for nano structured transparent $MgAl_2O_4$. Ceram Int 43:15352–15359. https://doi.org/10.1016/j.ceramint.2017.08.075
30. Ghosh SR, Mukherjee S, Banerjee S (2020) Development of spinel magnesium aluminate by solution combustion route using thiourea and urea as. Fuel J Eng Res [TJER] 17:135–141. https://journals.squ.edu.om/index.php/tjer/article/view/3680
31. Mukherjee S (2022) Development of spinel magnesium aluminate by modified solid state process and its characterization. Mater Today Proc 67:314–319. https://doi.org/10.1016/j.matpr.2022.07.113
32. Bai N, Liu X, Li Z, Ke X, Zhang K, Wu Q (2021) High-efficiency TiO_2/ZnO nanocomposites photocatalysts by sol–gel and hydrothermal methods. J Sol-Gel Sci Technol 99:92–100. https://doi.org/10.1007/s10971-021-05552-8
33. Khan AA, Javed M, Rauf Khan A, Iqbal Y, Majeed A, Hussain SZ, Durrani SK (2017) Influence of preparation method on structural, optical and magnetic properties of nickel ferrite nanoparticles. Mater Sci 35:58–65. https://doi.org/10.1515/msp-2017-0006
34. Enhessari M, Lachini SA (2019) $CuMn_2O_4$ nanostructures: facial synthesis, structural, magnetical, electrical characterization and activation energy calculation. Int J Bio Inorg Hybr Nanomater 8:39–45
35. Sanjabi S, Obeydavi A (2015) Synthesis and characterization of nanocrystalline $MgAl_2O_4$ spinel via modified sol–gel method. J Alloys Compd 645:535–540
36. Akbar N, Javed M, Arif Khan A, Masood A, Ahmed N, Mehmood RY, Khisro SN, Abdul MAS, Mohammad Haniff MAS, Shah A (2023) Zircon-type $CaCrO_4$ chromite nanoparticles: synthesis, characterization, and photocatalytic application for sunlight-induced degradation of rhodamine B. ACS Omega 8:30095–30108. https://doi.org/10.1021/acsomega.3c02457
37. Javed M, Khan AA, Akbar N, Kazmi J, Dar A, Mohamed MA (2023) Low-temperature dielectric relaxation mechanism and correlated barrier hopping transport in neodymium perovskite chromite. Mater Res Bull 165:112303. https://doi.org/10.1016/j.materresbull.2023.112303
38. Javed M, Akbar N, Khan AA, Alsubhe E, Mohammad Alghamdi S, Karamti H, Albeydani OA, ben Ahmed S, Kazmi J, Khisro SN, Mohamed MA (2023) Photocatalytic activity of sol-gel self-combustion derived MCr_2O_4 (M= Mg, Ni) spinel chromites for photodegradation of organic dyes. Mater Today Commun 35:105716. https://doi.org/10.1016/j.mtcomm.2023.105716
39. Li F, Zhao Y, Liu Y, Hao Y, Liu R, Zhao D (2011) Solution combustion synthesis and visible light-induced photocatalytic activity of mixed amorphous and crystalline $MgAl_2O_4$ nanopowders. Chem Eng J 173:750–759. https://doi.org/10.1016/j.cej.2011.08.043
40. Banerjee S, Mukherjee S, Ghosh SR (2021) Evaluation of properties of non-stoichometric alumina magnesia spinel using thiourea as fuel by varying soaking time. J Eng Res [TJER] 18:44–51. https://doi.org/10.53540/tjer.vol18iss1pp44-51
41. Javed M, Khan AA, Khisro SN, Majeed A, Kazmi J, Bilkees R, Hussain M, Mohamed MA (2022) Charge conduction mechanism and non-debye type relaxation in $LaCrO_3$ perovskite orthochromite. Mater Chem Phys 290:126522. https://doi.org/10.1016/j.matchemphys.2022.126522
42. Javed M, Arif Khan A, Kazmi J, Akbar N, Ahmed N, Khisro SN, Mohamed MA (2023) Investigation on electrical transport and dielectric relaxation mechanism in $TbCrO_3$ perovskite orthochromite. J Alloys Compd 955:170181. https://doi.org/10.1016/j.jallcom.2023.170181
43. Nassar MY, Ahmed IS, Samir I (2014) A novel synthetic route for magnesium aluminate ($MgAl_2O_4$) nanoparticles using sol–gel auto combustion method and their photocatalytic properties, Spectrochim. Acta A Mol Biomol Spectrosc 131:329–334. https://doi.org/10.1016/j.saa.2014.04.040
44. Ewais EMM, El-Amir AAM, Besisa DHA, Esmat M, El-Anadouli BEH (2017) Synthesis of nanocrystalline MgO/$MgAl_2O_4$ spinel powders from industrial wastes. J Alloys Compd 691:822–833. https://doi.org/10.1016/j.jallcom.2016.08.279
45. Goswami B, Rani N, Vats R, Bhukkal C, Ahlawat R (2021) Highly crystalline and narrow bandgap $MgAl_2O_4$: synthesis and characterization. In: AIP Conference Proceedings, AIP Publishing, p 020045. https://doi.org/10.1063/5.0052473
46. Abbasi Asl E, Haghighi M, Talati A (2020) Enhanced simulated sunlight-driven magnetic $MgAl_2O_4$-AC nanophotocatalyst for efficient degradation of organic dyes. Sep Purif Technol 251:117003. https://doi.org/10.1016/j.seppur.2020.117003
47. Kaur M, Pal K (2019) Review on hydrogen storage materials and methods from an electrochemical viewpoint. J Energy Storage 23:234–249. https://doi.org/10.1016/j.est.2019.03.020

48. Gholami T, Pirsaheb M (2021) Review on effective parameters in electrochemical hydrogen storage. Int J Hydrogen Energy 46:783–795. https://doi.org/10.1016/j.ijhydene.2020.10.003
49. Sangsefidi FS, Salavati-Niasari M (2017) Thermal decomposition synthesis, characterization and electrochemical hydrogen storage characteristics of Co_3O_4–CeO_2 porous nanocomposite. Int J Hydrogen Energy 42:20071–20081. https://doi.org/10.1016/j.ijhydene.2017.05.127
50. Salehabadi A, Salavati-Niasari M, Gholami T (2018) Green and facial combustion synthesis of $Sr_3Al_2O_6$ nanostructures; a potential electrochemical hydrogen storage material. J Clean Prod 171:1–9. https://doi.org/10.1016/j.jclepro.2017.09.250
51. Samimi F, Ghiyasiyan-Arani M, Salavati-Niasari M (2022) Synthesis of calcium manganese oxide with different constructions as potential materials for electrochemical hydrogen storage. Fuel 321:124074. https://doi.org/10.1016/j.fuel.2022.124074
52. Zhu H, Cao Y, Zhang J, Zhang W, Xu Y, Guo J, Yang W, Liu J (2016) One-step preparation of graphene nanosheets via ball milling of graphite and the application in lithium-ion batteries. J Mater Sci 51:3675–3683. https://doi.org/10.1007/s10853-015-9655-z